PERFORMANCE OF THE GUTENBERG-RICHTER LAW IN NUMERICAL AND LABORATORY EXPERIMENTS

Riera, J.D.[1] and Iturrioz, I.[2]
[1]Department of Civil Engineering, UFRGS, Porto Alegre, RS, Brazil <jorge.riera@ ufrgs.br>
[2]Department of Mechanical Engineering, UFRGS, Porto Alegre, RS, Brazil

ABSTRACT

The activity of fault sources is typically estimated from paleo-seismological and geomorphological investigations, whereas for area sources the activity is determined by statistical analysis of earthquakes catalogues in the region. The probability distribution of magnitude is then assumed to follow a doubly-bounded exponential distribution for area sources, which is a modified form of the famous Gutenberg-Richter equation. For fault sources, a characteristic distribution is often used, a special case of which is the maximum magnitude model. A justification of the ubiquitous GR law on physical grounds has been sought with limited success. On the other hand, during compression tests on concrete or rock specimens, the statistical analysis of acoustic emission (AE) signals emerging from the growing microcraks constitutes an effective damage assessment criterion. It has been observed that the signals amplitudes are distributed according to the GR law, and characterized through the *b*-value, which decreases systematically with damage growth. In experimental studies, AE signals are captured by sensors on the external surfaces of specimens subjected to compression. Test specimens were also analyzed using a 3D Discrete Element Method (DEM) lattice model by numerical simulation. The simulation closely reproduced the experimental results, not only in terms of stress-time global response, but also in terms of typical AE parameters, such as AE count rate, cumulative counts, and *b*-value variations. Using the DEM model, the relation between AE signals magnitude and the energy released in each localized rupture were also analyzed. The results are compatible with the GR energy-magnitude relation. Finally the numerical simulations present the same tendency observed in laboratory tests, which show a perceptible shift to lower AE frequencies during the evolution of the damage process. These promising results suggest that some features of the probability distribution of earthquake magnitudes may be correlated to the evolution of the damage process for the source under consideration and that these features may be assessed using numerical models.
.

INTRODUCTION

A justification of the ubiquitous Gutenberg-Richter (*GR*) law on physical grounds has been sought in Seismology with partial success. On the other hand, during laboratory compression tests on concrete or rock specimens, the statistical analysis of acoustic emission (*AE*) signals emerging from growing micro-cracks has recently shown that the amplitudes of the signals are distributed according to the *GR* law and characterized through its *b*-value, which decreases systematically with damage growth. The authors reviewed available field and laboratory evidence on the subject, presenting numerical simulations obtained by means of the Discrete Element Method (*DEM*) (Riera & Iturrioz, 2012). Herein those results are examined further, suggesting that some features of the probability distribution of earthquake magnitudes may be correlated with the evolution of the damage process for the source under consideration and that the geometric features of the causative faults may be resorted to in order to establish the maximum potential earthquake.

MAGNITUDE - FREQUENCY RELATION

The well-known *GR* expression for the relative frequency of seismic events larger than magnitude M_S suggested by Gutenberg and Richter (1954), has proved to be applicable in a surprising variety of geological and geographical locations:

$$Log_{10}\, N\,(\,M_S\,) = a - b\,M_S \tag{1}$$

The linear relation (1) presents a generally satisfactory fit to available global data, both for clearly identifiable seismogenic sources as well as for diffused seismicity regions. From equation (1) it follows that the probability of occurrence of an event of magnitude equal or larger than M_S is given by:

$$\text{Prob}\,[M_S \geq m] = \exp\,(-\beta\,m\,) \tag{2}$$

$$\beta = b\,ln\,10 \tag{3}$$

Thus, the *GR* frequency relation implies an exponential distribution of seismic magnitudes. In real situations, an upper limit is often imposed, defining the largest earthquake m_{max} that is considered possible for a specific seismogenic source. To account for the associated uncertainty in m_{max} , a probability distribution may be adopted, rather than a determined value. Similarly, a lower bound m_{min} may also be specified, which is in this case associated to the smallest event of engineering interest. In the presence of bounds, the relation between the yearly number N of seismic events larger than m results:

$$N(m)= v_{min}\,\{\,exp[-\beta\,(m - m_{min})] - exp[-\beta\,(m_{max} - m_{min})]\,/\,[\,1 - exp[-\beta\,(m_{max} - m_{min})]]\} \tag{4}$$

In which β is also defined by equation (3) and v_{min} denotes the number of events larger than m_{min} per year. In order to improve the fit of the magnitude-frequency relation to observed data, other models were suggested in the literature:

$$Log\ \ N\,(\,M_S\,) = a + b\,M_S - c\,M_S^2 \tag{5}$$

$$Log\ \ N\,(\,M_S\,) = a - b\,M_S + Log\,(\,c - \ M_S\,) \tag{6}$$

$$Log\ \ N\,(\,Log\,M_S\,) = a + b\,Log\,M_S - c\,(Log\,M_S\,)^2 \tag{7}$$

In equation (5) it is assumed that M_S is characterized by a log-normal probability distribution. Esteva (1976) argues that *G-R* equation (1) does not satisfactorily fit data that contain magnitudes above M_S= 7, proposing for such cases a double exponential function. A revision of statistical methods to estimate the *b*-coefficient in GR law as well as its associated uncertainty is due to Marzocchi and Sandri (2003). A single function, following Esteva`s arguments, based on the hypothesis that *G-R* law is valid for *low and for high magnitudes, but with different parameters in both regions,* with a smooth transition defined by the logistic function $f(M_S)$, has been employed by Riera (2009):

$$Log\,N\,(\,M_S\,) = [(a_1 - b_1\,M_S)\ \ f(M_S) + [(a_2 - b_2\,M_S)\,[1\text{-}f(M_S)] \tag{8}$$

$$f(M_S) =\ \ exp[-(M_S - M_C)/s]\,/\{\ 1+ exp[-(M_S - M_C)/s]\ \} \tag{9}$$

In addition to the doubly truncated *G-R* law given by equation (4), which is assumed applicable to small magnitude events, its combination with the so-called *Characteristic Earthquake* model, has also been suggested for cases in which a fault generates large earthquakes at intervals that are shorter than predictions based on the observation of small events. (Schwartz and Coppersmith, 1984; Youngs and Coppersmith, 1985; Wesnousky, 1994). Note that in the group of models reviewed by Bommer & Stafford (2008), the models described by equations (5) to (9) are not mentioned.

RELATIONS BETWEEN MAGNITUDE AND FAULT PROPERTIES

According to the Elastic Dislocation Theory, seismic events are due to shear failures, the seismic moment M_o being defined as (Abe, 1975):

$$M_o = \mu\,D\,A \tag{10}$$

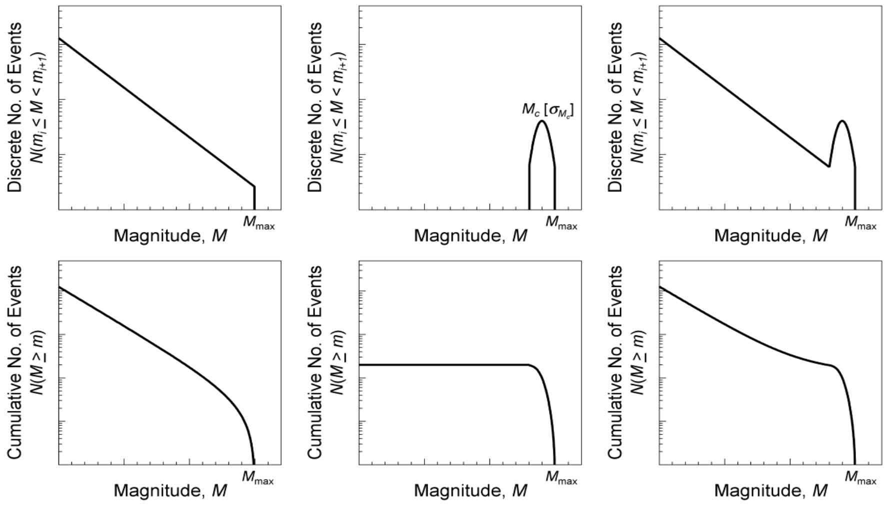

Figure 1. Typical recurrence relations, not-cumulative (above) and cumulative (below).
From left to right: Gutenberg-Richter model, maximum magnitude model and characteristic earthquake model (Bommer and Stafford, 2008).

In eq. (10) D denotes the mean displacement on the failure plane. Moreover, eq.(11) relates the seismic moment to the rupture area A and the average stress drop $\Delta\tau$:

$$M_o = C\,A^{3/2}\,\Delta\tau \tag{11}$$

The numerical coefficient C depends on the shape of the rupture surface, on the distribuition of applied stresses and on the degree of anisotropy of the medium. Typically, C varies between 0.6 and 0.75, its actual value being different for each seismic event. In the static approach, the parameters that describe the fault mechanism are its length L and width B, the shear modulus of the material μ and the seismic moment M_o , which are related by simple expressions. The mean stress $E(\tau)$ is needed to assess the change in strain energy ΔW caused by a seismic event. A fraction of this energy ΔW, known in Seismology as *seismic efficiency,* is irradiated in the form of seismic waves. The irradiated energy may also be quantified in terms of the mean stress drop $\Delta\tau$. Basic relations between these parameters were given by Kanamori and Anderson (1975). The Moment Magnitude scale M_w proposed by Hanks and Kanamori (1979) is defined as:

$$M_w = \tfrac{2}{3}\,log_{10}\,M_o - 10.7 \tag{12}$$

In which M_o is expressed in dyne×cm (10^{-7} Nm). Expression (12) has been adopted by the USGS for large US earthquakes since 2002. Moreover, the Moment Magnitude M_w is currently the preferred scale in ground motion prediction equations (*GMPE*) or in earthquake Catalogs. Expressing A and $\Delta\tau$ metric units and substituting eq.(11) into (12), leads to:

$$M_w = log_{10}A + \tfrac{2}{3}\,log_{10}\,\Delta\tau - 6{,}147 \tag{13}$$

While it is obvious that $\Delta\tau$ cannot exceed a fraction of the shear (or frictional) strength of rock, no similar physical restriction can normally be determined for the rupture area A in order to establish the upper bounds M_{max} shown schematically in Fig. (1) for specific cases of interest. On the other hand, this is not the case in laboratory specimens, as will be discussed later. In connection with field data, Wells and Coppersmith (1994) fitted the following equations to data grouped by the type of faulting:

$M_w = 1.02\ log_{10}A + 3.98$ (strike-slip) (13a)
$M_w = 0.90\ log_{10}A + 4.33$ (reverse) (13b)
$M_w = 1.02\ log_{10}A + 3.93$ (normal) (13c)
$M_w = 0.98\ log_{10}A + 4.97$ (all) (13b)

Papazachos *et al* (2004) established for strike-slip faults the following relations between M_w and the area A or fault rupture length L in km, respectively:

$M_w = 1.21\ log_{10}A + 3.37$ (strike-slip) (13e)
$M_w = 1.69\ log_{10}L + 3.90$ (strike-slip) (13f)

It is worth underlining that an extensive study has been conducted by EPRI (1994) in order to estimate M_{max} in Stable Continental Regions (*SCR*), based on statistics of past events collected worldwide, which aims at circumventing the typical lack of data in *SCRs*. In these regions, if seismogenic faults can be identified, an estimation of the largest possible rupture area jointly with eqs. (13) may serve as a complement to statistical approaches to assess M_{max}.

JUSTIFICATION OF FREQUENCY RELATIONS ON PHYSICAL GROUNDS

Numerous attempts have been made, with limited success, to explain on physical principles the satisfactory fit of *GR* or similar relations to observed seismic data. The subject still constitutes a promising area of research. Scholz (1968) examined the relation of the process of microfracturing in rocks observed in laboratory specimens with the frequency distribution of earthquakes. Bak and Tang (1989), following a theoretical approach, interpret the *GR* relation as a manifestation of *self-organized criticality* – (SOC), which has its fundaments in the Theory of Fractals. The approach was extended by Ito and Matsuzaki (1990), who develop a model to explain some seemingly fractal properties of seismic events, such as the potential distribution function of the size of earthquakes.

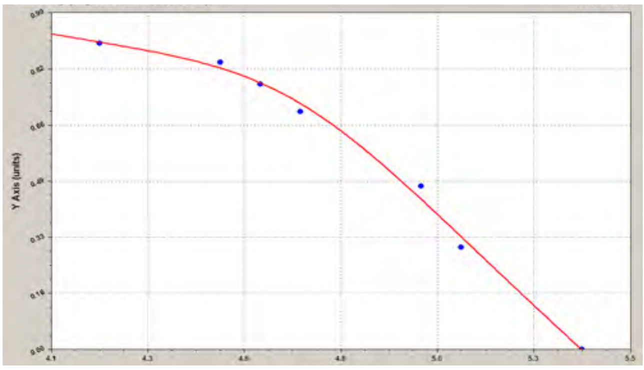

Figure 2. Fit of eqs. (9) to data from various sources in 70600km^2 low seismicity area in a stable continental region (SCR), in which M_C = 4.7 and s = 0.2, b_1= 0.2603 and b_2 = 1.0227.

Carpinteri *et al* (2009) examined recently, employing acoustic emission (*AE*) techniques, the applicability of *GR* relation in the ruptures process of concrete samples in laboratory tests in which they detected an evolution of the value of the *b*-coefficient from 1.5 to 1, as the system passes from the critical pre-failure state to final collapse. This decrease of the *b*-coefficient, also observed in laboratory samples by Scholz (1968, 2002), does not reproduce the *increase* in earthquake frequency vs. magnitude relations for entire regions, in which for lower magnitudes the slope b_1 in eq. (9) is always smaller than b_2. In fact, Scholz (2002) argues that, from the size distribution of sub-faults, it follows that $b_1 = ⅔$, while $b_2 = 1$, values that present a surprising universality. On the other hand, the coefficient $b = ⅔$ that would fit data for small earthquakes, say with $M_S < 3$ originated along a single fault, would likely underestimate the magnitude of a large earthquake from the same seismogenic source.

Figure 2 shows a typical example of data for various sources in a 70600km^2 low seismicity area in a stable continental region (SCR), in which $M_C = 4.7$, $s = 0.2$, $b_1 = 0.2603$ and $b_2 = 1.0227$. As is often the case, the slope *b* in the high magnitudes region is close to 1, although the slope in the low magnitude region is about a third of the theoretical value $b_1 = ⅔$ previously indicated. Almost invariably, seismic data leads to curves characterized by *increasing* negative slopes as the magnitude increases.

ACOUSTIC EMISSION: NUMERICAL AND EXPERIMENTAL RESULTS

Illustrative experimental results, as well as numerical simulations of laboratory tests aimed at the determination of the *b* value on small scale rock or concrete samples are described next. Information on fundaments and performance of the lattice formulation of the Discrete Element Method (DEM) proposed by Riera (1984), employed in the numerical analyses reported below, may be found in Kosteski *et al* (2011). The Acoustic Emission (AE) tests examined herein were reported by Carpinteri *et al* (2009). The first test consists of a 160×160×500mm concrete prism subjected to uniaxial compression. The laboratory specimen was modeled by means of a 27×27×86 DEM cubic modules array, with the boundary conditions shown in Figure 5.b. The parameters adopted in the DEM model with a perfect cubic mesh are: Young´s modulus of the material E=9.0 GPa, mass density ρ=2500Kg/m2, mean value of the material toughness $\mu(G_f)$=560N/m and the linear elastic limit strain $\varepsilon_p = 2.4\times10^{-4}$. The random nature of the material is taken into account by assuming the toughness as a random field with a coefficient of variation CV= 0.5. The value of the concrete modulus E=9GPa was adopted on account of the fact that the test sample was subjected during 48 hours to a uniform compression load of 1300 kN, then unloaded. During the ensuing test the damaged specimen was reloaded up to its final collapse, while monitored by AE sensors. Figure 5b shows the location of the AE sensor, at which accelerations in the direction normal to the specimen surface were computed employing the DEM.

The second example consists of a three point bending test. The concrete specimen dimensions were (80×150×700mm) with a 30mm pre-fissure length in the middle. The AE sensor was mounted as indicated by the gray box in Fig. 6b. Material properties were $E=35GPa$, ρ=2500Kg/m2, mean value of the toughness $\mu(G_f)$=130N/m and linear elastic limit strain $\varepsilon_p = 6.4\times10^{-5}$. Additional details concerning the experiments are biven by Carpinteri *et al* (2009, 2009b). The non-homogeneous nature of concrete is also taken into account in the numerical simulations by assuming that the toughness is a 3D random field with CV= 0.25. The applied displacement rates on numerical DEM models were reduced until no inertial effects could be detected in the output.

Figure 3 shows load vs. time diagrams measured in the experiments and determined herein by numerical simulation. The peak loads and the areas under the curves are similar in both examples, except for the loss of linearity of the experimental curve for uniaxial compression near the peak load, which suggests that large damage occurred before the peak, effect that is not observed in the numerical analysis. The load vs. time diagrams of both controlled displacement tests are quite different: in the compression test an explosive collapse occurs, while in the three point bending test a softening branch after the peak load is reached can be seen. The normalized energy balance in both tests determined by numerical simulation can be found in Riera and Iturrioz (2012). In the uniaxial compression test, 95% of the external work is available in the form of elastic energy when the final collapse occurs, resulting in an explosive failure. On the other hand, in the three point bending test the external work is smoothly dissipated during the entire process and the available potential energy at the end of the test is not sufficient to produce an explosive collapse. The final rupture configurations observed in the experimental setup and predicted numerically can be seen for the uniaxial compression test in Figure 4 and for the Three Point Bend test in Figure 5.

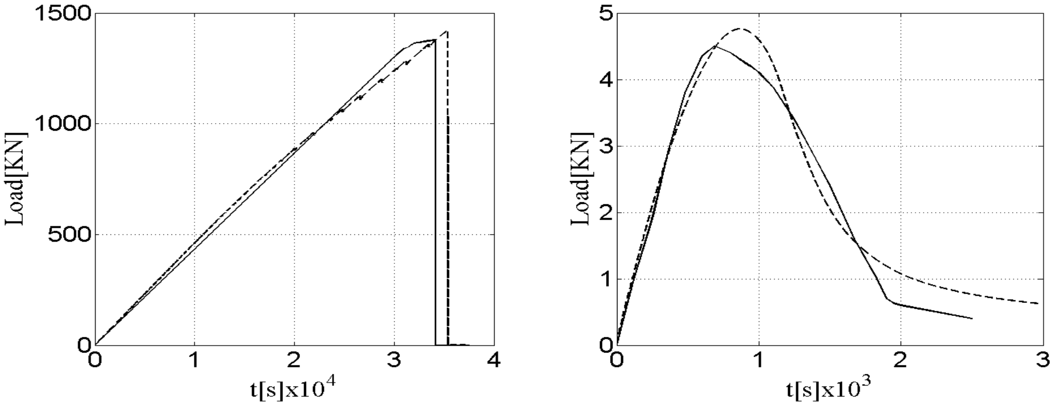

Figure 3: Load vs. time functions determined experimentally (continuous lines) and numerically (dashed lines): (a) Uniaxial compression test, (b) The three point bending test.

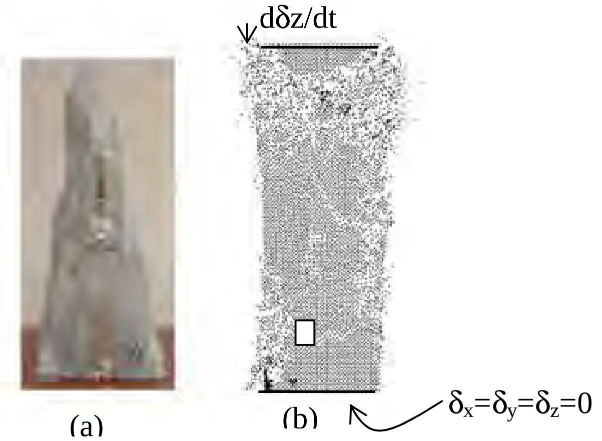

Figure 4. (a) Final rupture configuration of concrete specimen subjected to uniaxial compression (Carpinteri *et al*, 2009) and (b) collapse configuration predicted by DEM model after peak load is reached (only nodal masses are shown). The white rectangle indicates the position of the sensor.

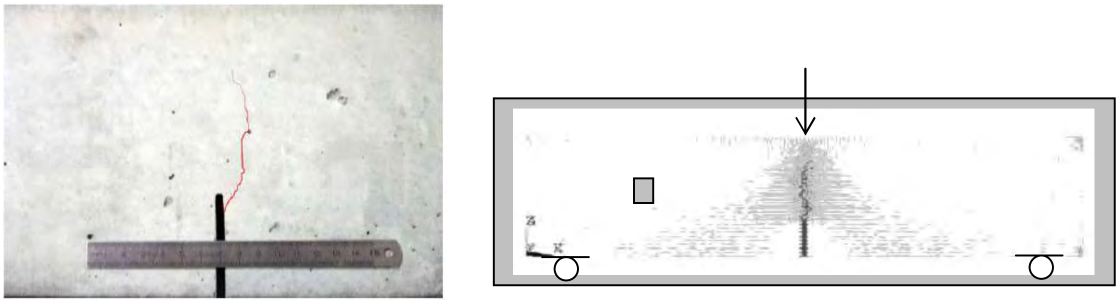

(a) (b)

Figure 5: (a) Detail of the exerimental rupture configuration of the specimen subjected to Three Point Bending (Carpinteri *et al*, 2009a) (b) Numerical rupture configuration according to DEM (only damaged bars are plotted). The small gray rectangle indicates the position of the sensor.

A summary of numerical results concerning Acoustic Emission (*AE*) for both tests is presented next. *AE* signals in the numerical simulations are defined as the accelerations normal to the surface, at points on the specimen where sensors were placed during the experiments. Figure 6 shows the occurrence of individual AE events as vertical bars on the time axis. The height of each bar is propotional to the intensity of the event, registered on the sample surface. The figure also shows the total load vs. time curves. Histograms of the number of AE events and the evolution with time of the accumulated number of events are shown in Figure 8 for the uniaxial compression test and for the three points bending test.

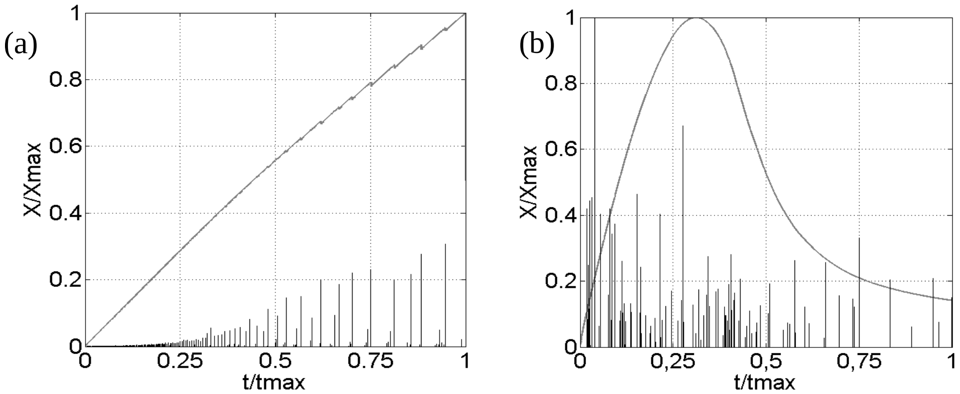

Figure 6 : Continuous curves indicate the total load in the DEM models, while the bars show the amplitudes of AE events. Both axis were normalized to the maximum value. (a) Uniaxial compression test, (b) Three points bending

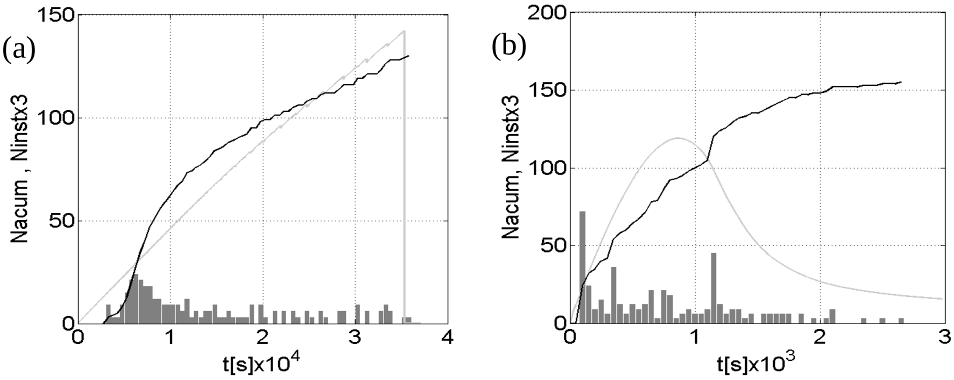

Figure 7 : Histograms of the number of AE events and evolution with time of accumulated number of events (thick line) and load evolution (thin line) for: (a) Uniaxial compression test, (b) Three points bending test.

Finally Figure 9 shows the relations between the number of AE events and their magnitudes in logarithmic scale. Straight lines were fitted to the simulated data within selected time intervals, as indicated in the graphs. The magnitude scale was normalized. All the signals utilized for the *b*-values calculation in the numerical simulation had higher amplitudes than the fixed threshold a_{thres}. For this reason, only few events were identified in the simulation (about 200 in each example). By decreasing even further the displacement rate and adopting a lower threshold, it would be possible to identify more AE peaks, thus increasing the sample size, but this longer analysis was considered unnecessary. The values of *b* computed in both examples are compatible with the values determined experimentally by Carpinteri *et al* (2009, 2009b). In addition, the numerical simulations reproduced the tendency observed in laboratory experiments, which show that *b* decreases towards values around unity as the degree of damage increases. In the uniaxial compression test the *b* value was observed to decrease from 1.69 to 1.19, while according to DEM predictions it decreases from 1.47 to 1.16. In the laboratory bending test, *b* decreases from 1.49 to 1.11, while the numerical simulation predicts a decrease from 1.10 to 1.03.

Figure 10 presents plots of the logarithm of the number of events larger than given amplitudes vs. the logarithms of the amplitudes for the DEM simulations of the compression test (left plot) and of the three points bending test (right plot). Notice that the shape of these curves are similar to the typical curve for seismic data shown in Fig. 2, which according to Scholz (2002), from the size distribution of sub-faults, may be expected to present slopes given by b_1= ⅔ and b_2= 1. While similar values are usually found in actual seismic records for specific faults or seismic regions, they differ from some of the laboratory or numerical simulations results for small samples discussed herein. For instance, equations (2.9) fitted to the data in Fig. 10, lead to b_1= 0.64 and b_2= 2.40 for the compression test and to b_1= 0.24 and b_2= 1.16 for the bending test.

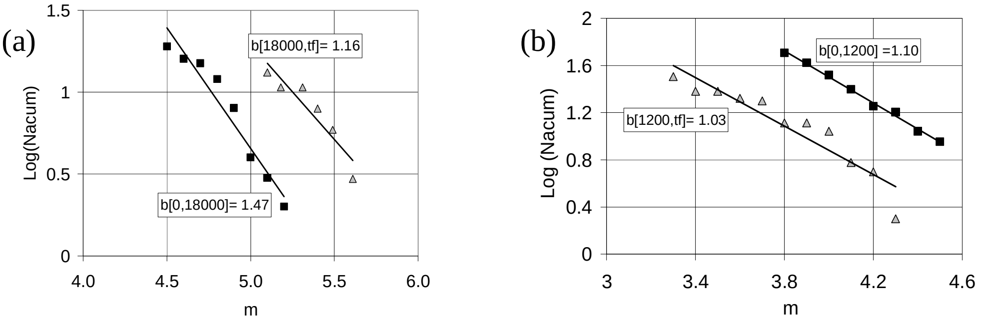

Figure 8: Determination of *b* - coefficients for simulated response in (a) uniaxial compression test and (b) three point bending test. The time intervals used in the computation of *b* values are indicated between brackets.

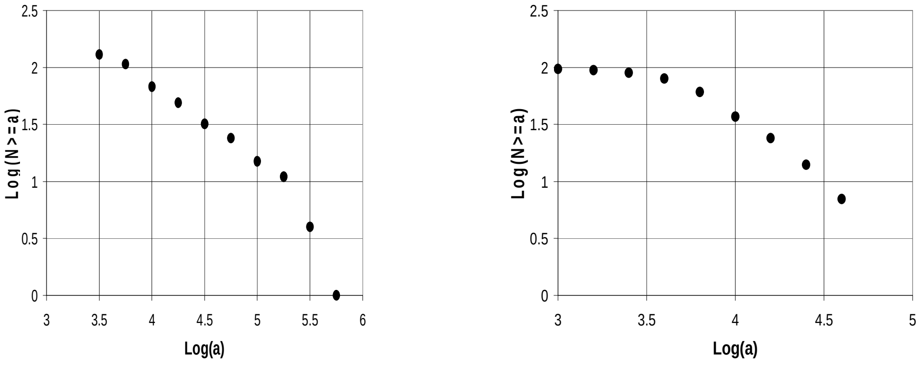

Figure 9: Logarithm of the number of events with amplitudes larger than a vs. the logarithm of a for DEM simulations of compression (left) and of three points bending (right). The *b* values in the high magnitudes regions are b_2= 2.40 (compression) and b_2= 1.16 (bending).

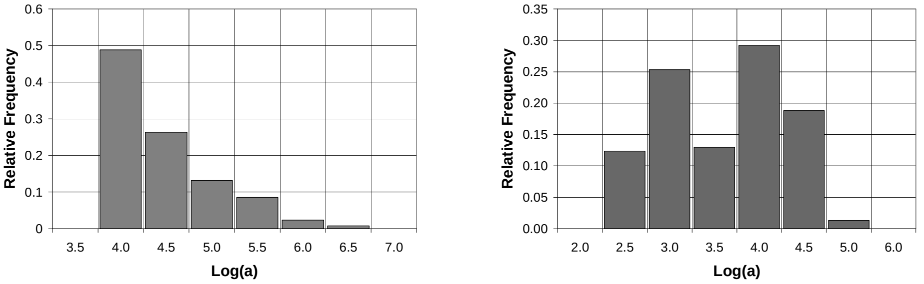

Figure 10: Histograms of the relative frequency of the logarithm of events amplitudes in AE numerical simulations, (left) compression test left, (right) three points bending test.

Fig. 10 above shows histograms of the relative frequencies of the logarithm of the amplitude of events in AE simulations, which has a strong similarity with the magnitude, as a measure of the size of seismic events, for the compression test (left) and three points bending (right). It is considered that the compression test, in which the failure mechanism is governed mainly by indirect tension and shear, would be a more appropriate model for examining the phenomenon of seismic rupture. The relation between the maximum size of the fracture that causes vibrations of amplitude *a* and the size of the tested sample is presently being studied. The analogy is further illustrated by Fig. 11, which shows the frequency distribution of seismic magnitudes, represented as *Log (a)*, of seismic events registered in a 400 km radius circular region centered at the Angra dos Reis NPP, Brazil, between 1961 and 2012, *i.e.* during approximately a 50 years period. The existence of an upper limit for the magnitude, clearly hinted by the results of small scale laboratory experiments and implicit in all probability distributions shown in Fig.1, cannot be inferred from Fig. 11, but remains a plausible assumption.

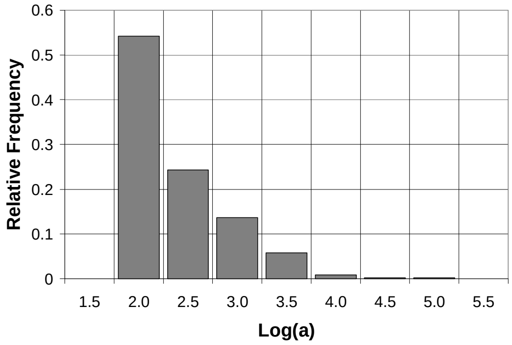

Fig. 11. Histogram of m_b seismic magnitudes of events in a 500 km radius circular area in a 50 years period in a SCR

CONCLUSIONS

A decrease of the slope *b* was observed both in laboratory experiments on small samples, as well as in numerical simulations of these tests, is interpreted as due to increasing damage in the medium. In seismic frequency vs. magnitude curves, the slope *b* typically decreases as the magnitude increases. The latter, however, are generally plots of the *collected data* for the available time of observation, while the former refer to successive *periods of observation*. A direct consequence of the previous observations would be that if seismic records for events at a given fault or well defined seismic region were separated in bins, say 500 years long, fits of the *GR* relation (2.1) to the separated data *should* present *b* values that decrease with time, that is, higher values for the older bins.

Another difficulty in comparing actual seismic data with laboratory simulations is related to the manner in which foreshocks and aftershocks are considered in the elaboration of seismic catalogues. In laboratory or numerical simulations every *AE* event is counted, without any attempt to identify clusters of events. Moreover, analysis of *AE* signals of large magnitude events shows that they typically mask the simultaneous occurrence of smaller events (originated at different sources) triggered by the former. These results suggest that some features of the probability distributions of earthquake magnitudes may be correlated with the evolution of the damage process for the source under consideration and that these features may be assessed using numerical models currently under development.

ACKNOWLEDGEMENTS

The authors acknowledge the support of CNPq and CAPES, Brazil.

REFERENCES

Abe, K. (1975): "Reliable estimation of the seimic moment of large earthquakes", *J. Physiks Earth Planet. Int.*, **23**, p. 381-390.

Bak, P. and Tang, C. (1989): "Earthquakes as a self-organized physical phenomenon", *Journal of Geophysical Research,* **94**, 15635-15637.

Bommer, J.J. and Stafford, P.J. (2008): "Seismic hazard and earthquake actions". *In*: *Seismic Design of Buildings to Eurocode 8,* A.Y. Elghazouli *ed.*, Taylor and Francis, 6-46.

Carpinteri, A., Lacidogna, G, Puzzi, S.(2009): "From criticality to final collapse: evolution of the *b*-value from 1.5 to 1.0". *Chaos, Solitons and Fractals*, **41**, 843–853.

Carpinteri, A., Lacidogna G., Niccolini G. (2009): "Fractal analysis of damage detected in concrete structural elements under loading". *Chaos, Solitons and Fractals*, **42**, 2047–2056.

Cornell, C.A. and Vanmarcke, E.H. (1969): "The major influences on seismic risk", *Proceedings of the Fourth World Conference on Earthquake Engineering*, Santiago de Chile, Vol. 1, A-1, 69-93.

EPRI (1994): "The Earthquakes of Stable Continental Regions", *EPRI TR 102261s* – Vols. 1-4.

Esteva, L. (1976): "Seismicity" , Chapter 7, in *Seismic Risk in Engineering Decisions,* Edited by C. Lomnitz and E. Rosenbluth, Elsevier Scientific Publications, London.

Gutenberg, B. and Richter, C.F. (1954): "Seismicity of the Earth and Associataed Phenomena", Princeton University Press, Princeton, NJ, USA.

Hanks, T.C. and Kanamorri, H. (1979): "A moment magnitude scale", *J.of Geophysical Research,* **84**, 2348-2352.

Ito, K. and Matsuzaki, M. (1990): "Earthquakes as self-organized critical phenomena", *Journal of Geophysical Research,* **95**, (B5) 6853-6860.

Kanamori, H. and Anderson, D.L. (1975): "Theoretical bases of some empirical relations in Seismology", *Bulletin of the Seismological Society of America, BSSA,* **65**, No. 5, pp. 1073, 1095.

Kosteski L., Iturrioz I., Batista R.G., Cisilino A. P.: "The truss-like discrete element method in fracture and damage mechanics". *Engineering Computations*, 2011; 6: 765–787.

Marzocchi, W. and L. Sandri (2003): "A review and new insigths on the estimation of the *b*-value and its uncertainty", *Annals of Geophysics,* **46**, No. 6, pp. 1271-1282.

Papazachos B. C., Scordilis E. M., Panagiotopoulos D. G., Papazachos C. B. and Karakaisis, G. F. (2004):"Global relations between fault parameters and moment magnitude of earthquakes", Bulletin of the Geological Society of Greece, Vol. XXXVI, 1482-1489.

Riera J. D.(1984): "Local effects in impact problems on concrete structures". *Proceedings,* Conference on Structural Analysis and Design of Nuclear Power Plants, Porto Alegre, RS, Brasil, 1984; Vol. 3,CDU 264.04:621.311.2:621.039.

Riera, J.D. and Iturrioz, I. (2012): "The Gutenberg-Richter and similar laws and their relation with numerical and experimental laboratory results", 15th World Conf. on Earth. Eng.", Paper 5827, 15WCEE, Lisboa, Portugal.

Scholz C. H. (1968): "The frequency- Magnitude Relation of Microfracturing in rock and its relation to earthquakes". Bull of the Seism. Soc of America, Vol 58 n1 pp399-415.

Scholz, C.H. (2002). The Mechanics of Earthquakes and Faulting, 2nd. Edition, Cambridge Univ. Press.

Schwartz, D.P. and K.J. Coppersmith (1984). "Fault behavior and characteristic earthquakes - examples from the Wasatch and San-Andreas fault zones". *Journal of Geophysical Research,* **89**, 5681-5698.

Wells D.L. & Coppersmith K.J. (1994)."New empirical relationships among magnitude, rupture length, rupture width, rupture area and surface displacement". Bull. Seism. Soc. Am., 84, 974-1002.

Wesnousky, S.G. (1994): "The Gutenberg-Richter or characteristic earthquake distribution, which is it?", *Bulletin of the Seismological Society of America-BSSA,* **84** (6), 1940-1959.

Youngs, R.R. and Coppersmith, K.J. (1985): "Implications of fault slip rates and earthquake recurrence models to probabilistic seismic hazard estimates". *Bulletin of the Seismological Society of America - BSSA*, **75**, 939-964.